Crystal Structure of Human Type III 3α-Hydroxysteroid Dehydrogenase/Bile Acid Binding Protein Complexed with $NADP^+$ and Ursodeoxycholate[†,‡]

Yi Jin,[§,||] Steven E. Stayrook,[||,⊥] Ross H. Albert,[⊥] Nisha T. Palackal,[⊥] Trevor M. Penning,*[,§] and Mitchell Lewis[⊥]

Department of Pharmacology, Department of Biochemistry and Biophysics, and The Johnson Research Foundation, University of Pennsylvania School of Medicine, Philadelphia, Pennsylvania 19104

Received May 4, 2001; Revised Manuscript Received June 28, 2001

ABSTRACT: The crystal structure of human type III 3α-hydroxysteroid dehydrogenase (HSD)/bile acid binding protein (AKR1C2) complexed with $NADP^+$ and 3α,7β-dihydroxy-5β-cholanic acid (ursodeoxycholate) at 3.0 Å resolution is presented. Thus, the three-dimensional structure has now been solved for a human HSD member of the aldo-keto reductase superfamily. AKR1C2 is implicated in the prostatic production of the potent androgen 5α-dihydrotestosterone and the hepatic transport of bile acids. It also catalyzes the formation of the neurosteroid 3α-hydroxy-5α-pregnan-20-one in the central nervous system, and its allosteric modulation by fluoxetine has been linked to the use of this drug for premenstrual dysphoria. Like other members of the superfamily, AKR1C2 folds into an α/β-barrel and binds $NADP^+$ in an extended conformation. The carboxylate of ursodeoxycholate binds to AKR1C2 in the oxyanion hole at the active site. More interestingly, the orientation of ursodeoxycholate is essentially "backwards" and "upside-down" from that observed for testosterone in the related rat 3α-HSD·$NADP^+$·testosterone ternary complex, where testosterone assumes the position of a 3-ketosteroid substrate. The orientation of ursodeoxycholate is thus similar to that expected of a 17β-HSD substrate. The ternary structure explains the ability of AKR1C2 to catalyze 3α-, 17β-, and 20α-HSD reactions. Comparison of the steroid binding pocket of AKR1C2 with that of rat 3α-HSD reveals significant differences in the positions of conserved and nonconserved loop residues, providing insights into the structural basis for the functional flexibility that is observed in all the human 3α-HSD isoforms but not in the rat isoform.

3α-Hydroxysteroid dehydrogenases (3α-HSDs;[1] EC 1.1.1.213) of the aldo-keto reductase (AKR) superfamily are cytosolic, monomeric oxidoreductases that interconvert 3-ketosteroids to 3α-hydroxysteroids (*1*−*3*). Four human 3α-HSD isoforms exist and perform diverse functions such as the hepatic clearance of steroid hormones, the transport and biosynthesis of bile acids, the regulation of androgen metabolism, and the formation of neurosteroids. These enzymes include human type I 3α-HSD (AKR1C4), type II 3α-HSD (AKR1C3), type III 3α-HSD (AKR1C2), and 20α-(3α)-HSD (AKR1C1). They share >83% sequence identity at the amino acid level.

Recent in vitro characterization of the homogeneous human recombinant 3α-HSD isoforms indicates that in addition to their 3α-HSD activity they also display varying degrees of 17- and 20-ketosteroid reductase activity and 17β- and 20α-hydroxysteroid oxidase activity (Figure 1) (*2*). The k_{cat}/K_m values coupled with a tissue distribution profile are illuminative of the distinct physiological functions for each isoform.

AKR1C4 is hepatic-specific and responsible for the formation of the 5α/5β-tetrahydrosteroids for subsequent excretion. AKR1C3 is predominantly expressed in the prostate and reduces 5α-dihydrotestosterone (5α-DHT, a potent androgen) to 5α-androstane-3α,17β-diol (a weak androgen), but is incapable of the reverse reaction due to its high 17β-HSD oxidative activity (*2*, *4*). Also prominently expressed in the prostate, AKR1C2 is the only known 3α-HSD isoform that will convert 5α-androstane-3α,17β-diol to 5α-DHT, which implicates its involvement in the intracrine formation of 5α-DHT in this gland. Since high levels of 5α-DHT are linked to abnormal prostate growth (*5*), inhibition of AKR1C2 represents an attractive strategy for the clinical management of prostate cancer and benign prostatic hyperplasia (*3*).

Also known as human bile acid binding protein (*6*, *7*), AKR1C2 is unique among human 3α-HSDs in that it is potently inhibited by bile acids. Dissociation constants of AKR1C2 for bile acids are significantly lower than those of the other human bile acid binders, such as the glutathione

[†] This work was supported by NIH Grant DK 47015 and CA 90744 awarded to T.M.P.

[‡] Atomic coordinates have been deposited at the Protein Data Bank (PDB ID: 1IHI).

* To whom correspondence should be addressed at the Department of Pharmacology, University of Pennsylvania School of Medicine, 3620 Hamilton Walk, Philadelphia, PA 19104-6084. Tel: (215) 898-9445; Fax: (215) 573-2236; E-mail: penning@pharm.med.upenn.edu.

[§] Department of Pharmacology.

[||] Authors contributed equally to this work.

[⊥] Department of Biochemistry and Biophysics and The Johnson Research Foundation.

[1] Abbreviations: HSD, hydroxysteroid dehydrogenase; AKR, aldo-keto reductase (also visit www.med.upenn.edu/akr); AKR1C1, human 20α(3α)-HSD; AKR1C2, human type III 3α-HSD/bile acid binding protein; AKR1C3, human type II 3α-HSD; AKR1C4, human type I 3α-HSD; AKR1C8, rat 20α-HSD; AKR1C9, rat 3α-HSD; 5α-DHT, 5α-dihydrotestosterone; allopregnanolone, 3α-hydroxy-5α-pregnan-20-one; ursodeoxycholate, 3α,7β-dihydroxy-5β-cholanic acid.

10.1021/bi010919a CCC: $20.00
Published on Web 07/31/2001

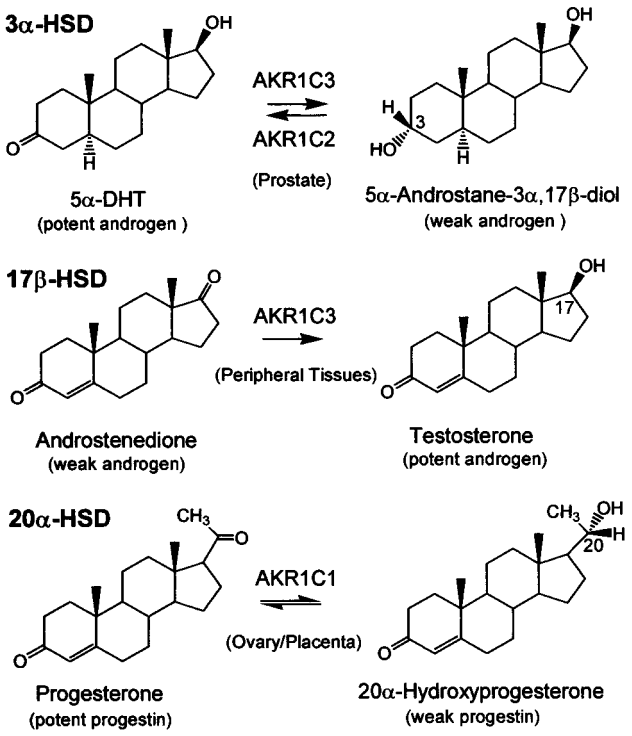

FIGURE 1: Representative 3α-, 17*β*-, and 20α-HSD reactions catalyzed by human 3α-HSDs. In each instance, there is the conversion of a potent steroid hormone to its cognate inactive metabolite. Substituents below the plane of the steroid are α-orientated (e.g., the C3 hydroxyl group in 5α-androstane-3α,-17*β*-diol) while substituents above the plane of the four rings are *β*-orientated (e.g., the C17 hydroxyl group in testosterone).

S-transferases and fatty acid binding proteins, suggesting its dominant role in intracellular bile acid transport (*8*).

In addition, AKR1C2 catalyzes the formation of 3α-hydroxy-5α-pregnan-20-one (allopregnanolone), an anxiolytic neurosteroid that is an allosteric effector of the GABAa receptor (*2*). Recently, it was suggested that AKR1C2 may be allosterically regulated by fluoxetine, which can increase allopregnanolone formation by lowering the K_m for 5α-dihydroprogestins (*9*). This may explain the use of this selective serotonin reuptake inhibitor in the treatment of premenstrual syndrome.

Remarkably differing from AKR1C2 by only seven amino acids (*7*), AKR1C1 is not inhibited by bile acids and is not implicated in either 5α-DHT or allopregnanolone formation. Rather it functions as a 20α-HSD and interconverts progesterone (an active progestin) with its inactive metabolite (20α-hydroxyprogesterone).

Virtually all mammalian 3α- and 20α-HSDs belong to the AKR superfamily with the best-characterized member being the rat liver 3α-HSD (AKR1C9) (*10*). This enzyme is the only 3α-HSD isoform in rat and shares 69% sequence identity with the human isoforms. It is catalytically more efficient than human 3α-HSDs, but lacks 17*β*- or 20α-HSD activities. Although the available crystal structures of AKR1C9 and its complexes have provided clues to the structure−function relationships for HSDs of the AKR family (*11*−*13*), they fail to explain the observed difference in the affinity for bile acids and how some isoforms can function as 17*β*- and 20α-HSDs.

We now report the crystal structure of AKR1C2 in complex with $NADP^+$ and 3α,7*β*-dihydroxy-5*β*-cholanic acid

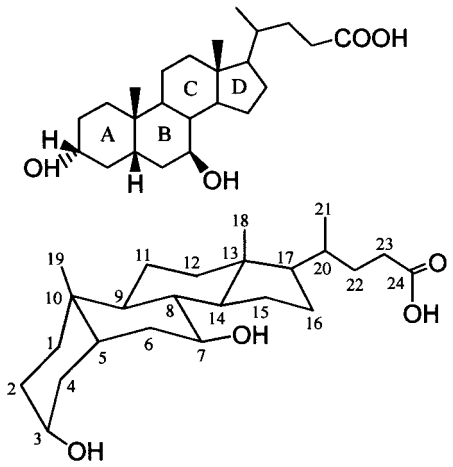

FIGURE 2: Structure of ursodeoxycholate. The four rings in the steroid are designated A, B, C, and D. The lower panel shows the bent structure between rings A and B due to the *β*-orientated hydrogen at the C5 position.

(ursodeoxycholate, Figure 2). It is the first structure of a human HSD member of the AKR superfamily and is pertinent to other human isoforms due to their high homology. The structure reveals the basis of the binding of bile acids to AKR1C2. Since ursodeoxycholate is a potent competitive inhibitor for AKR1C2, an understanding of its binding interaction will aid the rational design of isoform-specific inhibitors. The structure also provides insight into the functional flexibility of human 3α-HSDs.

EXPERIMENTAL PROCEDURES

Protein Purification and Crystallization. Recombinant AKR1C2 was overexpressed in *E. coli* and purified to homogeneity as described (*14*). The enzyme was dialyzed into 10 mM potassium phosphate buffer, pH 7.0, containing 1 mM EDTA and 1 mM 2-mercaptoethanol, and concentrated to 20 mg/mL. The ternary complex of AKR1C2 was prepared by the addition of a 10-fold excess of $NADP^+$ (final concentration 5 mM) to the concentrated enzyme, followed by further dialysis against the same buffer containing 0.2 mM ursodeoxycholate and cosolvent (5% ethanol). Crystals of diffraction quality were grown at 22 °C by the hanging-drop vapor diffusion method using 23% PEG 5000 MME, 100 mM sodium cacodylate, pH 6.0, and 200 mM ammonium sulfate. The concentration of PEG 5000 MME was increased to 25%, and glycerol (16%) was added for cryogenic freezing.

Data Collection and Structure Determination. X-ray diffraction data were collected from a single crystal at 100 K using an 18 cm MAR Research image plate mounted on a Siemens M18X rotating anode generator employing a Charles Supper mirror system. The data were processed with DENZO (*15*). Equivalent measurements were scaled using SCALEPACK and merged with an overall R_{merge} of 5.2% (10.2% in the outer shell)(Table 1). Crystals were of *R*32 symmetry with unit cell parameters of $a = b = 144.09$ Å, $c = 202.75$ Å, $\alpha = \beta = 90°$, $\gamma = 120°$. There were two protein molecules in the asymmetric unit.

The structure of the AKR1C2 ternary complex was solved by molecular replacement using AMORE (*16*) with reflection data from 10 to 4 Å and an integration radius of 25 Å. Coordinates of a single protein molecule of the AKR1C9·

Table 1: Data Collection and Refinement Statistics

resolution range (Å)	8.0−3.0
total reflections	99026
unique reflections	16424
completeness (%)	99.8
R_{merge}[a] (%)	5.2
$I/\sigma(I)$	20.3
R_{cryst},[b] R_{free}[c] (%)	22.3, 27.8
average *B*-value (Å^2)	15.8
root-mean-square deviations	
bond lengths (Å)	0.009
bond angles (deg)	1.5
dihedral angles (deg)	23.3
improper angles (deg)	0.9

[a] $R_{merge} = \Sigma\Sigma|I - \langle I\rangle|/\Sigma\Sigma I$, where I is the observed intensity and $\langle I\rangle$ is the average intensity over all observations of symmetry-related reflections. [b] The crystallographic R factor, defined as $\Sigma||F_o| - |F_c||/\Sigma|F_o|$, where $|F_o|$ and $|F_c|$ are the observed and calculated structure factor amplitudes, respectively. [c] The free R factor, calculated from the randomly chosen 10% of the reflections (the test set) that were not included in atomic refinement.

NADP$^+$·testosterone ternary complex (PDB entry: 1AFS) (*13*) were used as the search model. The two molecules in the asymmetric unit were found by a sequential search. The top solution, which gave 37% correlation and an R factor of 49%, showed reasonable packing between symmetry-related molecules in the unit cell and provided a starting point for refinement.

Model Building and Refinement. The model was manually rebuilt using the program O (*17*) and refined using the program CNS (*18*). Coincident with reductions in the values of the free R factor and the crystallographic R factor, the electron density was gradually clarified by cycles of manual adjustment and refinement and two rounds of molecular averaging and solvent flattening. The improved map revealed defined density near the active site residues suitable for the cofactor and the bile acid. Subsequently, structures of NADP$^+$ and ursodeoxycholate [retrieved from the Cambridge database (*19*)] were introduced into the model and refined. Tight noncrystallographic 2-fold symmetry restraints or strict constraints were used in the refinement and were gradually loosened and released at the final stage of the refinement. The two protein molecules in the asymmetric unit appear to be identical in structure and share the same ligand occupancy and ligand geometry. For each molecule, 2 N-terminal residues and 1 C-terminal residue out of the 323 residues of the protein were not included due to lack of electron density. The geometry of the model was assessed by PROCHECK (*20*).

RESULTS AND DISCUSSION

Overall Structure of the AKR1C2·NADP$^+$·Ursodeoxycholate Ternary Complex. The protein structure of AKR1C2 displays the characteristic fold of the AKR superfamily (*21*): an $(\alpha/\beta)_8$ barrel with three associated large loops (Figure 3). The β-strands ($\beta1-\beta8$) form the cylindrical core of the barrel and are surrounded by α-helices (α1−α8), while the accompanying loops (A, B, and C) partially cover the C-terminal end of the barrel. In addition to the $(\alpha/\beta)_8$ core structure, there are two β-strands (B1 and B2) from the N-terminus sealing the N-terminal end of the barrel and two α-helices (H1 and H2) from the C-terminal part of the molecule packed by the side of the barrel. These additional β-strands and α-helices are conserved in other AKR structures (*21*). NADP$^+$ and ursodeoxycholate bind in two different regions of the protein with the nicotinamide ring of the cofactor and the carboxylate of the steroid converging at the core of the barrel. Ursodeoxycholate is located in a deep cavity at the C-terminal end of the barrel, essentially parallel to the barrel axis, whereas NADP$^+$ extends across the barrel closer to the core and lies perpendicular to the steroid.

An overlay of the AKR1C2·NADP$^+$·ursodeoxycholate ternary complex with the AKR1C9·NADP$^+$·testosterone complex shows overall close similarity in structure. The average root-mean-square deviation of all 320 equivalent Cα positions between the 2 proteins is 0.8 Å with the largest displacements occurring in the N-terminal 6 amino acids. The positions of the cofactor and the active site residues are highly conserved, while notable differences exist in the loop structures involved in the binding of the steroid ligand.

Binding of Ursodeoxycholate to AKR1C2. The electron density for the ursodeoxycholate molecule is well-defined (Figure 4a). Ursodeoxycholate is an A/B-*cis*-ring fused (5β-H configuration) or "bent" steroid (Figure 2). This structural feature allowed the unambiguous placement of the molecule into the density, which showed a sharp angle suitable for the turn between the A and B rings of the steroid. No other orientation of the steroid could adequately account for the density.

Ursodeoxycholate occupies a large and elongated binding cavity formed by residues from six loops, the loop connecting β1 and α1 (the β1-α1 loop), the β2-α2 loop, the β3-α3 loop, Loop-A, Loop-B, and Loop-C. The bile acid molecule makes a large number of contacts with residues Tyr24, Val54, Tyr55, Trp86, His117, Val128, Ile129, Trp227, and Leu308 (Figure 4b). The binding interactions are highly hydrophobic in nature with the exception of interactions involving the carboxylate group and 7β-hydroxyl group. One end of the bile acid is anchored deeply in the cavity by interactions between the carboxylate moiety and the side chains of Tyr55 and His117. The body of the steroid is tethered at the 7β-hydroxyl group by a hydrogen bond to the side chain of Tyr24, which is in turn hydrogen-bonded to Glu224. The steroid is sandwiched between Val54 and Trp227 with the side chain of Val54 in close contact with the C18-methyl group on the β-face and the side chain of Trp227 opposing the α-face of the C and D rings of the steroid. In addition, side chains of Val128 and Ile129 make van der Waals contacts with the A and C rings of the steroid, while Trp86 and Leu308 interact with the C21 methyl group and C22, respectively.

Conserved NADP$^+$ Binding and Active Site Structure. NADP$^+$ is bound in an extended anti-conformation in the ternary complex of AKR1C2. The nicotinamide moiety is positioned at the core of the barrel structure by stacking against Tyr216 and forming a network of three hydrogen bonds between the carboxamide group and the side chains of Ser166 and Asn167. The pyrophosphate portion of NADP$^+$ is stabilized by hydrogen bonds and a salt bridge with residues Ser217, Leu219, Ser221, and Lys270, while the 2′-phosphate of the adenosine moiety is salt-linked or hydrogen-bonded to Lys270, Ser271, Tyr272, and Arg276. The latter interactions would favor the binding of NADP(H) over NAD(H). In addition, residues Tyr24, Asp50,

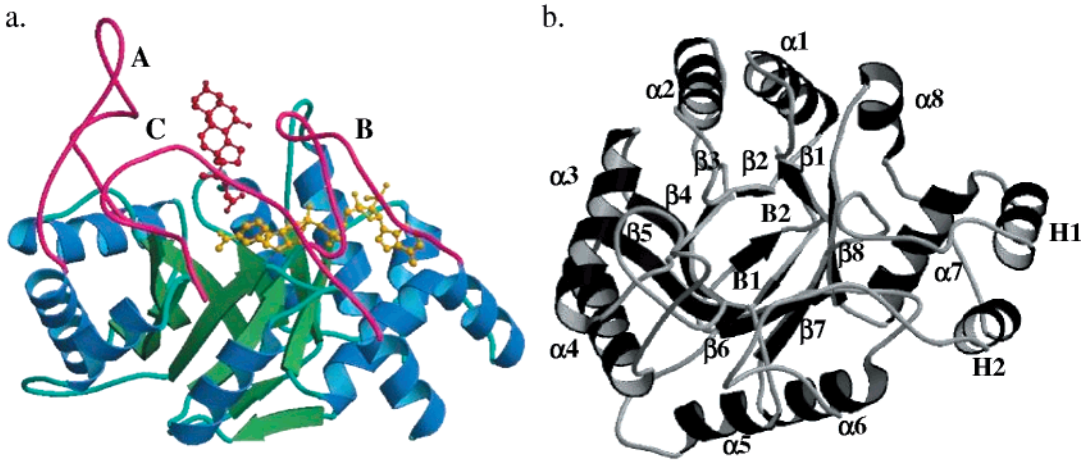

FIGURE 3: Overall structure of the AKR1C2 ternary complex. In panel a, the helices and the strands are colored in blue and green, and the three associated loops are in dark pink and labeled A, B, and C. The $NADP^+$ cofactor and ursodeoxycholate are show in ball-and-stick representation in gold and red, respectively. The view is perpendicular to the barrel axis. The secondary structural elements are labeled in panel b, with the view down the barrel axis from the top. The residue numbers in each segment are as follows: β1, 19−23; α1, 32−45; β2, 48−51; α2, 59−71; β3, 80−85; α3, 91−105; β4, 110−118; α4, 144−158; β5, 159−166; α5, 170−178; β6, 187−192; α6, 199−209; β7, 211−216; α7, 251−263; β8, 265−270; α8, 273−280; B1, 6−9; B2, 15−17; H1, 239−248; H2, 290−298. Figures 3−6 were prepared using MOLSCRIPT (*22*).

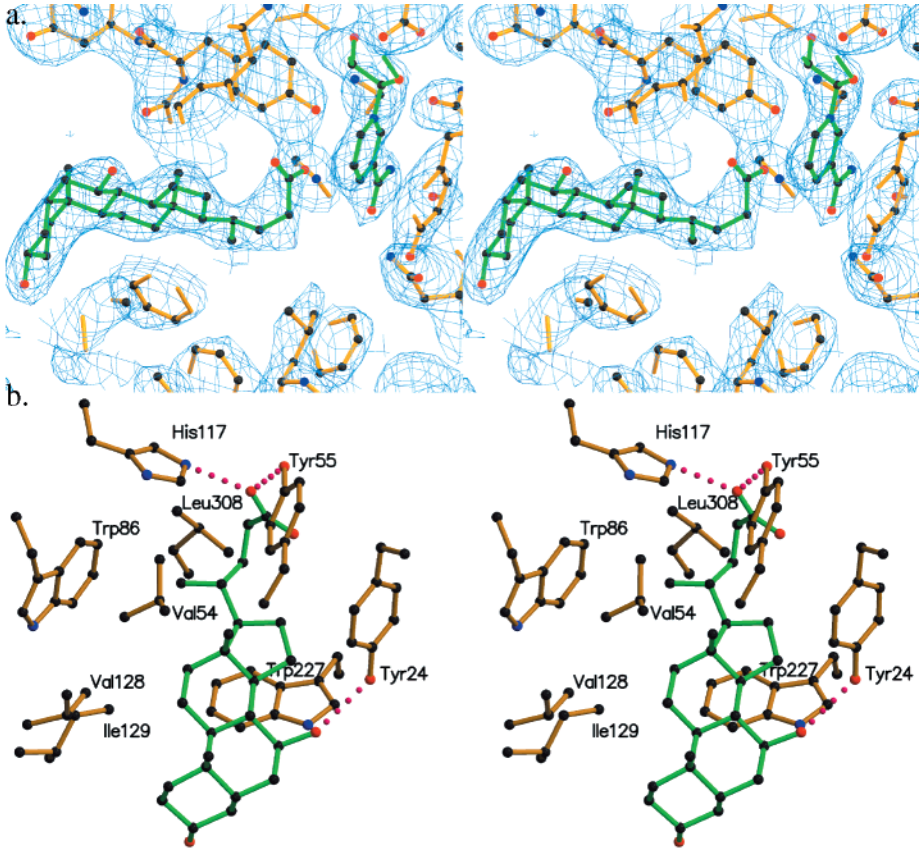

FIGURE 4: (a) Stereoview of the electron density at the steroid binding cavity of AKR1C2. The map was calculated with ursodeoxycholate excluded from the model, at 3 Å resolution with $2F_o-F_c$ amplitudes and model phases, contoured at 1 standard deviation. (b) Stereoview of the steroid binding cavity of AKR1C2. Shown in ball-and-stick representation, ursodeoxycholate and the cofactor are colored in green, and surrounding residues are colored in gold. All atoms are colored by atom type; black for carbon, blue for nitrogen, and red for oxygen. Hydrogen bonds between ursodeoxycholate and the enzyme are shown as dashed lines in dark pink.

Gln279, and Asn280 form hydrogen bonds with the ribose hydroxy oxygens and adenine ring nitrogens.

The binding mode of the cofactor in the ternary complex of AKR1C2 closely resembles those reported for the complexes of AKR1C9. The residues involved in interactions are highly conserved and perform similar roles. In fact, many hydrogen-bonding interactions between the protein and the cofactor appear to be conserved across the entire superfamily. However, like the complexes of AKR1C9, the AKR1C2 ternary complex lacks a salt-link 'safety-belt' found in members of the aldehyde reductase (AKR1A) and aldose reductase (AKR1B) subfamilies (*23*−*25*).

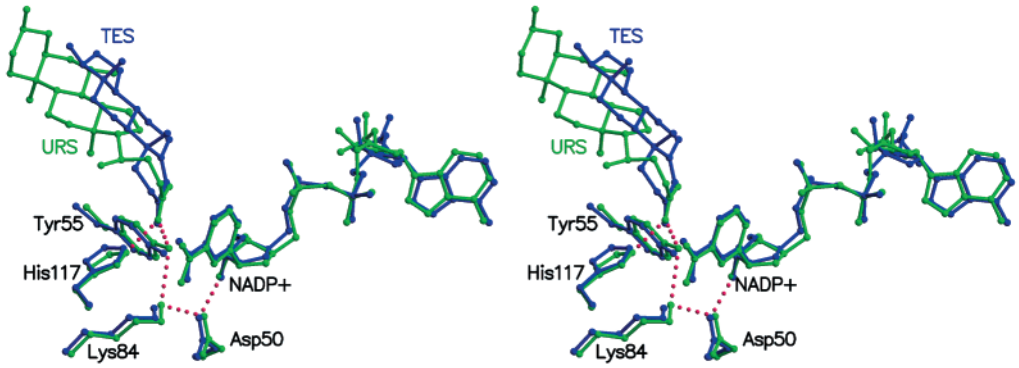

FIGURE 5: Comparison of active site structure and ligand binding in AKR1C2 (green) and AKR1C9 (blue). The two enzyme complexes demonstrate conservancy in the binding of the cofactor and the spacial arrangement of the catalytic tetrads. Functional groups of the inhibitors, C3-ketone of testosterone (TES) and C24-carboxylate of ursodeoxycholate (URS), also adopt identical spatial positions in the two active sites. Amino acid residues and ligands are shown in ball-and-stick representation. Hydrogen bonds are indicated as dashed lines in dark pink.

A similar degree of preservation was also observed in the active site of AKR1C2 and AKR1C9 (Figure 5). In the center of the active sites is Tyr55, which is involved in hydrogen-bond networks with residues Lys84 and H117 (via the steroid). Lys84, in turn, is salt-linked to Asp50. Known as the catalytic tetrad, these residues are essential for AKR1C9 catalysis (*26*). The tetrad, which is highly conserved throughout the AKR superfamily, has the identical spatial arrangement relative to the nicotinamide ring of the cofactor in the complexes of AKR1C2 and AKR1C9. It was anticipated that the carboxylate group of ursodeoxycholate would bind to the oxyanion hole formed by the tetrad of AKR1C2. Indeed, one carboxylate oxygen of ursodeoxycholate is in close proximity with the hydroxyl group of Tyr55, and the carboxylate carbon is in close proximity with the C4 of the nicotinamide ring of $NADP^+$. Similarly, the corresponding position in the active site of AKR1C9 was occupied by the C3 ketone of testosterone in the AKR1C9 complex. The functional groups of these competitive inhibitors thus occupy the same site as the reactive center of a steroid substrate during an enzymatic reaction.

Implications for Kinetic and Catalytic Mechanisms. All AKRs follow a sequential ordered bi-bi mechanism in which the cofactor binds first and leaves last (*10*). The binding and release of the cofactor are proposed to be the rate-determining steps for the overall catalysis of aldehyde and aldose reductases (*27*). The conformational rearrangements associated with the formation and disruption of the "safety-belt" upon cofactor binding and release are speculated to be related to the slowest step in the reaction. By contrast, the absence of the "safety-belt" in AKR1C2 and AKR1C9 may facilitate the conformational changes during cofactor association or dissociation. This agrees with kinetic studies on AKR1C9 in which the events associated with cofactor binding were found to be only partially rate-determining in the overall reaction (*28*).

The interactions for cofactor in the complexes of AKR1C2 and AKR1C9 are basically invariant, suggesting similar binding events with the two isoforms. AKR1C9 exhibits conformational changes in Loop-B upon cofactor binding (*12*, *13*). Similar loop movements are likely to occur with AKR1C2 at comparable rates. Thus, the differences in kinetic properties of the homologue, e.g., k_{cat} values 100-fold higher for AKR1C9 than AKR1C2, are likely to arise from the chemical events and/or events related to steroid binding or release.

Table 2: Sequence Alignments of Selected Regions in Several HSD Enzymes of the AKR Gene Superfamily[a]

	β1-α1	β2-α2	β3-α3	Loop-A	Loop-B	Loop-C
	24 25 26 27	54 55	86	117 118 128 129	224 225 226 227	306 307 308 309 310
AKR1C2	**Y** A P A	**V Y**	**W**	**H** F **V** **I**	E E P **W**	L T **L** D I
AKR1C1	Y A P A	L Y	W	H F V I	E E P W	L T L D I
AKR1C3	Y A P P	L Y	W	H S L S	D K R W	F N S D S
AKR1C4	Y A P P	L Y	W	H F P L	H K L W	V V M D F
AKR1C8	Y A T E	L Y	W	H F L L	Y K Y C	F P A N M
AKR1C9	**T** V P E	**L Y**	W	**H F** F **F**	D K **T** **W**	**N** N A K **Y**

[a] The secondary structure of each region is noted above the alignment. The residues of AKR1C2 and AKR1C9 that interact with the steroids are shaded and in boldface.

The chemical mechanism of the reaction involves acid−base catalysis (*26*). Direct hydride transfer of the 4-*pro-R* hydrogen of the cofactor to the ketone of the steroid is facilitated by a general acid. In the reverse reaction, a general base deprotonates the steroid alcohol to facilitate hydride transfer back to the cofactor. Site-directed mutagenesis on AKR1C9 suggests that Tyr55 functions as both the general acid and base (*26*). Its bifunctionality relies on contributions through hydrogen-bond networks from Lys84 and H117 that alter the pK_a and pK_b of Tyr55, respectively. The preservation of cofactor binding and active site structure suggests that AKR1C2 catalysis follows a similar "push−pull" mechanism.

Variant Steroid Binding Pockets and Different Steroid Binding Modes in AKR1C2 and AKR1C9. The steroid binding pockets of AKR1C2 and AKR1C9 are formed by residues from the same regions of the respective proteins (Table 2). Structural studies on AKR1C9 identified 10 residues involved in steroid binding (*13*). However, a partially different set of residues is responsible for the binding of ursodeoxycholate to AKR1C2. Comparison of the pockets reveals significant differences in the spatial positions and conformations of these residues with the exception of Tyr55 and His117 (Figures 5 and 6).

Sections of Loop-C (residues 306−311) display a large degree of sequence variation among the HSDs, and they

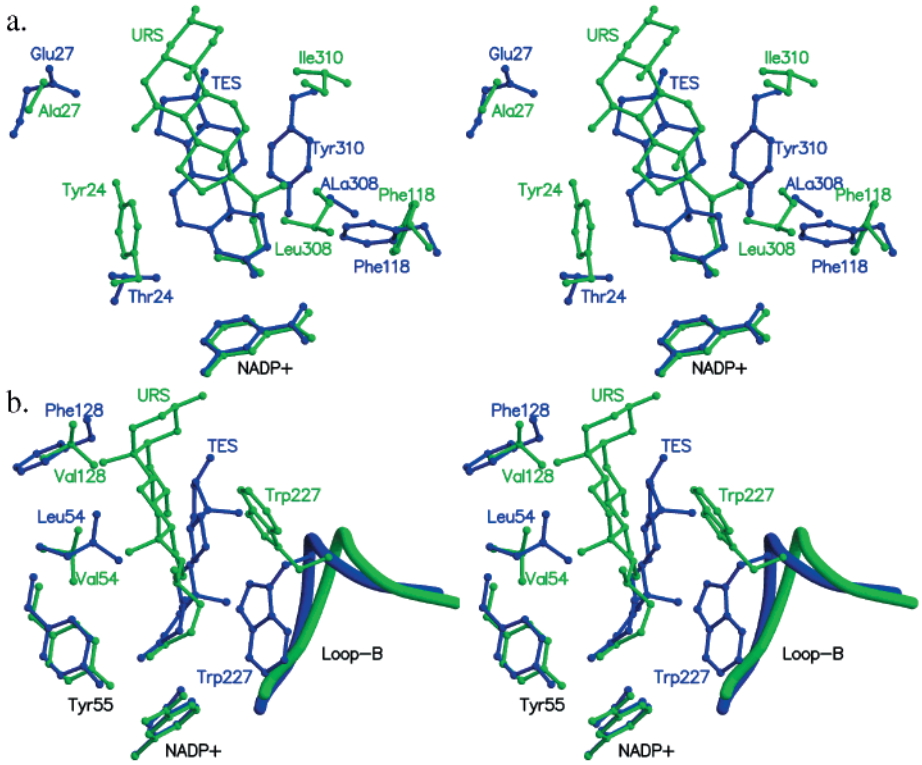

FIGURE 6: Comparison of the steroid binding cavities and the position and orientation of steroids in AKR1C2 (green) and AKR1C9 (blue). The steroid binding cavities of the two enzymes have different structures, and the steroids, testosterone (TES) and ursodeoxycholate (URS), assume opposing orientations. Amino acid residues, steroids, and the nicotinamide rings of the cofactors are shown in ball-and-stick representation. A section of Loop-B (residues 223−229) is shown in panel b. The view in panel b is rotated 90° about the vertical axis relative to panel a.

adopt different conformations in the ternary complexes of AKR1C2 and AKR1C9. Of these residues, the difference at 310 is most significant. Cα atoms of 310 residues are displaced by 2.5 Å between the 2 enzymes, with Tyr310 of AKR1C9 being closer to the center of the substrate pocket. Its large side chain projects toward the center of the steroid cavity and forms van der Waals contacts with the steroid rings (3.2 Å at the closest distance). By contrast, the corresponding residue in AKR1C2, Ile310, is not within contact distance (>6 Å) of ursodeoxycholate and may contribute to steroid binding only by maintaining the hydrophobicity of the pocket. Similarly, residues 25−27 of the β1-α1 loop also exhibit a large displacement in main chain positions (average 2 Å at equivalent positions). With the substitution of Ala for Glu at 27, the combined effect is to create a larger opening near the surface of AKR1C2.

Striking structural differences were also observed for some of the conserved residues that line the pocket. Trp227 of Loop-B is highly conserved among HSDs with the exception of rat ovary 20α-HSD (AKR1C8), but it is preceded by a region with the least conserved residues (amino acids 224−226). Significant displacements are seen in these residues with the positions of equivalent Cα atoms varying by up to 3.2 Å (at residue 226). Such changes in main chain locations may cause the difference in the position of Trp227 (Figure 6b). Compared to Trp227 of AKR1C9, which is in van der Waals contacts with the A and B rings of testosterone, the side chain of Trp227 in the AKR1C2 complex rotates approximately 120° and contacts the C and D rings of ursodeoxycholate. In addition, a different side chain conformation is observed for Phe118 of AKR1C2, a residue also highly conserved in HSDs of the superfamily (Figure 6a).

Little displacement is seen in the positions of main chain atoms of residues 24, 54, 128, and 129. However, substitution of Tyr for Thr at position 24 in AKR1C2 provides an important hydrogen-bonding interaction with the 7β-hydroxyl group of ursodeoxycholate.

In the two complexes, both testosterone and ursodeoxycholate are anchored at the oxyanion hole of the respective proteins. However, due to the difference in contours of the substrate cavities, the bodies of the steroids assume different locations within the pockets (Figure 6b). Most interestingly, the steroids adopt essentially opposite orientations in the two structures. Binding of the carboxyl group of ursodeoxycholate to the active site brings the D ring of the steroid proximal to Tyr55, resulting in a "backwards" position as compared to that of testosterone in AKR1C9. Ursodeoxycholate is also "upside-down" relative to testosterone in that the two angular methyl groups of the two ligands are inverted. As a result, in the two structures Loop-B lies against opposing faces of the steroid ring, i.e., the α-face of ursodeoxycholate and the β-face of testosterone.

Determinants of Inhibitor Sensitivity. The potent inhibition of AKR1C2 by ursodeoxycholate can now be explained. The bile acid molecule is tethered both at the carboxylate end and at the 7β-hydroxyl group by several hydrogen bonds, and it is positioned in the cavity such that numerous hydrophobic contacts are achieved. The binding of ursodeoxycholate at the active site of AKR1C2 supports the notion of using a negatively charged carboxylate group as an anchor in the design of inhibitors for this enzyme. However, the interactions at the active site are unlikely to be the sole determinants of the unique nanomolar affinity of AKR1C2 for bile acids since the oxyanion hole exists in all AKRs.

Of the residues contacting the bile acid molecule, Tyr24, Val54, and Trp227 appear to play a dominant role in the binding of ursodeoxycholate.

The position of Val54 in AKR1C2 explains why the identity of the residue at this position determines the functional difference between AKR1C1 and AKR1C2 as indicated by previous site-directed mutagenesis (*29*). Different in sequence at only seven positions, AKR1C1 prefers reactions at the C20 position and has a K_d for ursodeoxycholate 300-fold higher. The structure of AKR1C2 shows that replacement of Val54 by a Leu residue would bring the side chain carbons in clashing distance with the C18 angular methyl group of ursodeoxycholate. As a result, an alternative position and/or orientation would have to be adopted by the bile acid in AKR1C1, which would disrupt the stabilizing hydrogen-bonding interactions involving the 7β-hydroxyl group of the bile acid and Tyr24 and cause a decrease in affinity.

AKR1C9 also displays high affinity for bile acids, but like AKR1C1 it has a Leu at position 54. However, the aforementioned difference in the position of Trp227 makes it still possible for the bile acid to be sequestered between Leu54 and Trp227 and possibly be stabilized by hydrogen bonding with Thr24 of the rat enzyme.

Structural Basis for Functional Flexibility. In the AKR1C9·$NADP^+$·testosterone complex, the β-face of the steroid adopts an orientation that would permit the C3-ketone of a steroid substrate to be a recipient of the hydride ion to form a 3α-axial alcohol. A 3-ketosteroid substrate would assume a similar orientation in AKR1C2; i.e., the A-ring of the steroid would be proximal to the active site and its β-face would face Loop-B. Since the position and orientation of ursodeoxycholate in the AKR1C2 complex are essentially "backwards" and "upside-down" relative to those of testosterone in the AKR1C9 complex, the orientation of ursodeoxycholate in AKR1C2 reveals a steroid binding mode that could explain its 17β-HSD reactivity; i.e., the D ring of a 17-ketosteroid substrate would be proximal to the active site, and its α-face would face Loop-B. Since the position of the cofactor would be unchanged, this would permit hydride transfer to the α-face of the steroid at the 17-position, resulting in a 17β-equatorial alcohol. The structure supports the proposal that human 3α-HSDs are able to bind steroids in more than one orientation to achieve broad substrate specificity (*2*). The third possible orientation of a steroid substrate would be that for 20α-HSD activity which would require a 20-ketosteroid substrate to bind only "backwards", i.e., the D ring of the steroid proximal to the active site and its β-face facing Loop-B. All three binding modes must be allowed by AKR1C2 and other human isoforms to achieve their observed 3α-, 17β-, and 20α-HSD activity.

Although all human 3α-HSD isoforms (AKR1C1−4) display 17β-HSD and 20α-HSD reactivity to varying degrees, rat enzymes AKR1C8 and AKR1C9 are positional and stereospecific for 20α- and 3α-HSD reactions, respectively. AKR1C9 was converted into a positional and stereospecific 20α-HSD only after a loop-chimera approach in which all three loops (A, B, and C) of AKR1C8 were introduced into AKR1C9 (*30*). Comparison of the steroid binding pockets of AKR1C2 and AKR1C9 provides insights into the structural basis of the observed differences. The relatively large size of the substrate channel in AKR1C2 may allow the steroid some freedom to occupy several different orientations within the active site and still contact the hydrophobic residues that line the binding pocket. As a result, different residues are recruited for interaction when the steroid is positioned differently. By contrast, the steroid binding cavity of AKR1C9 limits the entry of substrates. Attempts at modeling substrates into AKR1C9 for 17β- and 20α-HSD reactions have revealed steric violation with surrounding residues, especially with Leu54, Trp227, and Tyr310.

The differences in steroid binding sites of AKR1C2 and AKR1C9 show that the fine-tuning of the steroid binding pocket to target steroid selectivity involves both using different amino acid side chains and changing the spatial position of main chain atoms. It indicates that the 10 residues identified previously as comprising the steroid pocket of AKR1C9 are not adequate predictors for steroid specificity by different HSDs in the same family. It is therefore not surprising that replacing only the residues in contact with testosterone failed to introduce 20α-HSD activity into AKR1C9 (*30*). These observations indicate that steroid-transforming AKRs alter the shape of their steroid binding sites and recruit different residues (conserved and nonconserved) for their steroid and inhibitor preferences.

REFERENCES

1. Penning, T. M., Bennett, M. J., Smith-Hoog, S., Schlegel, B. P., Jez, J. M., and Lewis, M. (1997) *Steroids 62*, 101−111.
2. Penning, T. M., Burczynski, M. E., Jez, J. M., Hung, C.-F., Lin, H.-K., Ma, H., Moore, M., Palackal, N., and Ratnam, K. (2000) *Biochem. J. 351*, 67−77.
3. Jin, Y., and Penning, T. M. (2001) *Best Pract. Res. Clin. Endocrinol. Metab. 15*, 79−94.
4. Lin, H.-K., Jez, J. M., Schlegel, B. P., Peehl, D. M., Pachter, J. A., and Penning, T. M. (1997) *Mol. Endocrinol. 11*, 1971−1984.
5. Gormley, G. J. (1991) *Urol. Clin. N. Am. 18*, 93−98.
6. Stolz, A., Hammond, L., Lou, H., Takikawa, H., Ronk, M., and Shively, J. E. (1993) *J. Biol. Chem. 268*, 10448−10457.
7. Hara, A., Matsuura, K., Tamada, Y., Sato, K., Miyabe, Y., Deyashiki, Y., and Ishida, N. (1996) *Biochem. J. 313*, 373−376.
8. Bahar, R. J., and Stolz, A. (1999) *Gastroentrol. Clin. 28*, 27−58.
9. Griffin, L. D., and Mellon, S. H. (1999) *Proc. Natl. Acad. Sci. U.S.A. 96*, 13512−13517.
10. Penning, T. M. (1999) *J. Steroid Biochem. Mol. Biol. 69*, 211−225.
11. Hoog, S. S., Pawlowski, J. E., Alzari, P. M., Penning, T. M., and Lewis, M. (1994) *Proc. Natl. Acad. Sci. U.S.A. 91*, 2517−2521.
12. Bennett, M. J., Schlegel, B. P., Jez, J. M., Penning, T. M., and Lewis, M. (1996) *Biochemistry 35*, 10702−10711.
13. Bennett, M. J., Albert, R. H., Jez, J. M., Ma, H., Penning, T. M., and Lewis, M. (1997) *Structure 5*, 799−812.
14. Burczynski, M. E., Harvey, R. G., and Penning, T. M. (1998) *Biochemistry 37*, 6781−6790.
15. Otwinowski, Z., and Minor, W. (1997) *Methods Enzymol. 276*, 307−326.
16. Navaza, J. (1994) *Acta Crystallogr. A50*, 157−163.
17. Jones, T. A., Zou, J.-Y., Cowan, S. W., and Kjeldgaard, M. (1991) *Acta Crystallogr. A47*, 110−119.
18. Brunger, A. T., Adams, P. D., Clore, G. M., Delao, W. L., Gros, P., Grosse-Kunstleve, R. W., Jinag, J.-S., Kuszewski, J., Nilges, M., Pannu, N. S., Read, R. J., Rice, L. M., Simonson, T., and Warren, G. L. (1998) *Acta Crystallogr. D54*, 905−921.
19. Higuchi, T., Kamitori, S., Hirotsu, K., and Takeda, H. (1985) *J. Pharm. Soc. Jpn. 105*, 1115−1118.

20. Laskowski, R. A., MacArthur, M. W., Moss, D. S., and Thornton, J. M. (1993) *J. Appl. Crystallogr. 26*, 283−291.
21. Jez, J. M., Bennett, M. J., Schlegel, B. P., Lewis, M., and Penning, T. M. (1997) *Biochem. J. 326*, 625−636.
22. Kraulis, P. J. (1991) *J. Appl. Crystallogr. 24*, 946−950.
23. Wilson, D. K., Bohren, K. M., Gabbay, K. H., and Quiocho, F. A. (1992) *Science 257*, 81−84.
24. Borhani, D. W., Harter, T. M., and Petrash, J. M. (1992) *J. Biol. Chem. 267*, 24841−24847.
25. El-Kabbani, O., Judge, K., Ginell, S. L., Myles, D. A. A., Delucas, L. J., and Flynn, T. G. (1995) *Nat. Struct. Biol. 2*, 687−692.
26. Schlegel, B. P., Jez, J. M., and Penning, T. M. (1998) *Biochemistry 37*, 3538−3548.
27. Grimshaw, C. E., Bohren, K. M., Lai, C. J., and Gabbay, K. H. (1995) *Biochemistry 34*, 14356−14365.
28. Ratnam, K., Ma, H., and Penning, T. M. (1999) *Biochemistry 38*, 7856−7864.
29. Matsuura, K., Deyashiki, Y., Sato, K., Ishida, N., Miwa, G., and Hara, A. (1997) *Biochem. J. 323*, 61−64.
30. Ma, H., and Penning, T. M. (1999) *Proc. Natl. Acad. Sci. U.S.A. 96*, 11161−11166.

BI010919A